ARMA 13-280

Significance of rock THM parameters in geological nuclear waste storage simulation

Dupray, Fabrice

École Polytechnique Fédérale De Lausanne (EPFL), School of Architecture, Civil and Environmental Engineering (ENAC), Laboratory for Soil Mechanics (LMS), Lausanne, Switzerland

Li, Chao

id.

Laloui, Lyesse

id., and King Abdulaziz University, Jeddah, Saudi Arabia

This paper was prepared for presentation at the 47th US Rock Mechanics / Geomechanics Symposium held in San Francisco, CA, USA, 23-26 June 2013.

ABSTRACT: A deep geological repository involving a multi-barrier system constitutes one of the most promising options to isolate high-level radioactive waste from the human environment. In order to certify the efficiency of waste isolation, it is essential to understand the behavior of the confining geomaterials under a variety of environmental conditions. The efficiency of an Engineered Barrier System (EBS) is largely based on a combination of bentonite and host rock characteristics. To contribute to a better understanding of the processes involved in the EBS, a case study for sensitivity analysis has been defined and is studied using a thermo-hydro-mechanical (THM) finite element approach including a consistent thermo-plastic constitutive model for unsaturated soils. The model also features a coupled THM approach of the water retention curve for bentonite, using the ACMEG-TS constitutive model. Regarding rock parameters, intrinsic permeability and relative permeability effects are evaluated. Two regimes are found regarding the importance of the estimation of rock permeability: in the first one, precise assessment is unnecessary due to water inflow control by bentonite, while in the second one, a precise assessment is necessary to correctly estimate resaturation time. This study highlights the effects that need to be taken into consideration for a correct assessment of EBS behavior, from bentonite characteristics to the correct quantification of the thermo-hydro-mechanical couplings in host rock.

1. INTRODUCTION

The fate of high-level radioactive waste is of a great importance to nuclear power plants operators and government agencies responsible for safety due to their extremely slow decay and the high risks associated with their management. Geological disposal is widely regarded as the safest option to alleviate any undue burden for future generations caused by this type of radioactive material [1]. This idea led to the development of the Engineered Barrier System (EBS) principle, which consists of using different layers of protection to insulate radioactive waste in all situations, from the short-term high-temperature situation to the very-long term scenario. Such a radioactive waste design makes use of a carefully chosen natural barrier (the so called host rock, even if host clays are also planned), as well as two additional layers of protection. One of these is the canister that contains the waste, which is fabricated from a metal, such as pure copper or a specific steel alloy. The second layer of protection is a buffer material that is designed to dissipate heat in a controlled manner to mitigate the risks from earth movements within the drift (host rock fracturation, seismic events) and to limit the possibility of radionuclide migration.

The aim of this paper is to identify the key parameters related to the host rock relevant for the design of the EBS. The description of the model focuses on the behavior of the buffer material, as this is the location of the most complex and physically coupled thermo-hydro-mechanical phenomena, but the interaction of the buffer with the host rock remains crucial in the development of these phenomena. The buffer material most commonly used in EBS designs is bentonite, either compacted as blocks or in pellet form [2, 3]. Although they behave differently, these two forms of bentonite share a large number of their main characteristics [4]; they both exhibit a very low permeability, a highly variable

thermal conductivity, an initial unsaturated state, and swelling characteristics.

The various processes that occur in the EBS are first outlined, with an emphasis on the coupled phenomena, as well as the necessary constitutive equations that describe them. This section includes the diffusive aspects (thermal and hydraulic behavior), as well as their coupling using a mechanical constitutive model. Next, the mechanical constitutive model used for the buffer is described, which is the ACMEG-TS model [5], an elasto-thermoplastic model that uses the framework of generalized effective stress for unsaturated soils, while the host rock is described as elastic. In the second section, a case study is described that is designed to represent a generic EBS design. This case study is simulated using the described constitutive equations in a finite element code. The results obtained for a base case are presented. Finally, results from some variations in the description of the host rock are analyzed and compared to the base case.

The case study under consideration is that of a single canister enclosed in a hole that is excavated without access drift. This choice allows the elimination of the site effects due to the drift and gives a better analysis of the effects of the modeling modifications. The geometry and heat dissipation are based on the Swedish proposal for an EBS [3], and the canister emits heat according to the decay of a real high-level waste canister. The geometry of the vertical deposition hole is shown in Fig. 1. As in the planned repositories, holes are excavated with a regular pattern, 400 m below the surface; therefore the modeled host rock radius is small (8.74 m) while a sufficient height is needed to avoid boundary effects (100 m).

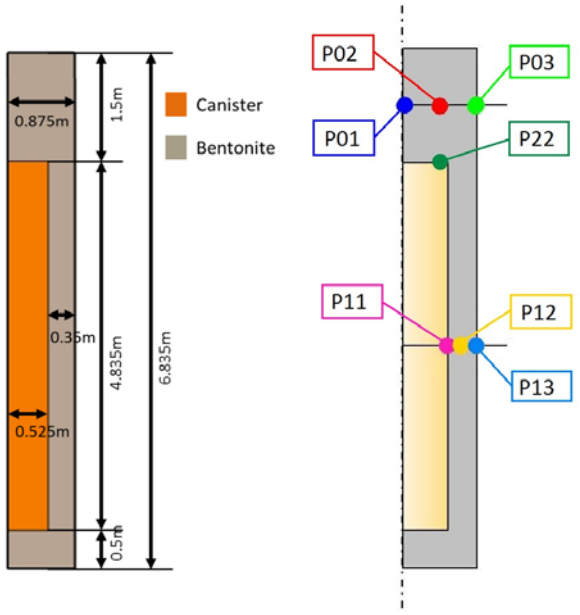

Fig. 1. Geometry of the considered deposition hole, location of monitoring points.

2. COUPLED PROCESSES IN AN EBS

2.1. Physical description

With the exception of the canister, the materials involved in the problem are porous media. The description of diffusive processes in such media have been treated with a variety of approaches such as the theory of mixtures [6], or the compositional approach which is used here. This approach separates species and phases into constituents for the mass balance equations, allowing a clear identification of the phase change quantity, which cancel out in the balance equations of the chemical species [7, 8]. The diffusive model presented in section 2.2 is used for both the host rock and bentonite buffer.

In order to understand the various processes involved, it is necessary to define the extreme conditions that are encountered. The temperatures considered in this study are between 15 and 80 °C, which is the design criteria for some EBSs [3]. The host rock is considered to be initially saturated, and acts as a permanent supply of water to the initially unsaturated buffer. The first two processes are thus an increase in temperature adjacent to the canister (diffusion of decaying radionuclide heat) and water exchange at the boundary between the saturated host rock and unsaturated buffer materials. The heat generated is thought to be capable of provoking further drying of the unsaturated buffer, as well as possibly the host rock. In terms of modeling, this implies that the water retention model should be able to reproduce the effect of temperature on the retention capacity.

Changes in liquid water content strongly influence the thermal conductivity, as well as the heat capacity, of the porous media. Bentonite is extremely affected by this phenomenon [9]. The degree of saturation will have a huge effect on the gas and liquid relative permeabilities of the porous medium. The diffusion of vapor created close to the canister should also be modeled, while the Richards' approximation is used to model vapor diffusion in a static gas phase; Wang et al. [10] demonstrated the use of this solution to provide good results in full-scale simulations. Convective heat flow can also be induced by fluid flows and should be taken into account, for both vapor and liquid water.

Thermo-hydro-mechanical couplings not only affect the diffusive part of the model, but also the mechanical one. The most well-known effects are the increase in strength that is induced by drying, and the changes in the swelling behavior at high temperatures [11]. These experimentally-observed effects are taken into account directly in the constitutive model and are detailed in section 2.3.

2.2. Coupled diffusive model

2.2.1. Water species

As stated previously, the compositional approach is used, as implemented by Collin et al. (Collin et al.,

2002) in the software Lagamine, that is also used for this study (Charlier et al., 2001). This approach allows writing the mass balance equation for water in a straightforward manner, including terms for storage of both liquid and gaseous water, advective flow of water, non-advective flow of vapor and source terms:

$$\underbrace{\frac{\partial}{\partial t}\left(\rho_w n S_r\right)+div\left(\rho_w \mathbf{f_l}\right)-Q_w}_{\text{Liquid water}}+\underbrace{\frac{\partial}{\partial t}\left(\rho_v n\left(1-S_r\right)\right)+div\left(\mathbf{i_v}\right)-Q_v}_{\text{Water vapour}}=0 \tag{1}$$

where ρ_w and ρ_v are the bulk density of liquid water and water vapor; $\mathbf{f_l}$ is the macroscopic velocity of the liquid phase; $\mathbf{i_v}$ is the non-advective flux of water vapor, itself the opposite of dry air flux; S_r is the degree of liquid saturation, and n the porosity. The term $\rho_w n S_r$ is the storage term for liquid water. No gas flow appears, as per Richards' approximation.

Among these terms, the liquid water flow is defined by the generalized Darcy's law for porous media:

$$\mathbf{f_l}=-\frac{k_{r,w}k_{int}}{\mu_w}\mathbf{grad}\left(p_w\right) \tag{2}$$

where p_w is the liquid water pressure, $k_{r,w}$ the relative permeability to water, k_{int} the intrinsic permeability and μ_w the dynamic viscosity of liquid water. The relationship between the relative permeability and degree of saturation is defined according to the properties of each material. The intrinsic permeability depends on porosity through a Kozeny-Carman relationship:

$$k_{int}=k_{int,0}\left[\frac{n/n_0}{\left(1-n\right)/\left(1-n_0\right)}\right]^{\eta} \tag{3}$$

where $k_{int,0}$ is the intrinsic permeability at the initial porosity n_0 and η is a material parameter. This relationship and the storage term in equation (1) define one side of the hydro-mechanical coupling.

As the vaporization/condensation term is not visible in the compositional approach, the thermo-hydraulic coupling does not appear as such in these relationships, and should be highlighted separately as appearing in several terms of equation (1). One element of this coupling is the evolution of the water properties with temperature, such as liquid density, but also dynamic viscosity. The dynamic viscosity of water is calculated through the relationship proposed by Thomas and King [12], which is valid for the range of temperatures considered here:

$$\mu_w=0.6612(T-229)^{-1.562} \tag{4}$$

where μ_w is the dynamic viscosity of water in Pa.s and T the temperature in Kelvin.

Liquid water is treated as a compressible and dilatant fluid, which is a correct assumption between 10 and 100 °C. The linearized relationship for the definition of liquid density is:

$$\rho_w=\rho_{w0}\left[1+\kappa_T\left(p_w-p_{wr}\right)-\beta_w\left(T-T_r\right)\right] \tag{5}$$

where κ_T is the isothermal water compressibility, β_w the volumetric thermal expansion coefficient of water and p_{wr} and T_r are the reference pressure and temperature, respectively.

The effect of temperature on water is more important when considering vaporization. It is interesting here to define the matrix suction as the difference between the gas pressure and (negative) water pressure, as $s=p_g-p_w$ (otherwise, when $p_w<p_g$, $s=0$). Vapor in the porous medium is supposed to be in thermodynamical equilibrium with liquid water, and, using Kelvin-Laplace's law as the definition of relative humidity h, the following relationship is obtained:

$$\rho_v=\rho_{v,sat}h=\rho_{v,sat}\exp\left(\frac{-s}{\rho_w R_v T}\right) \tag{6}$$

where R_v is the gas constant of water vapor, and $\rho_{v,\mathrm{sat}}$ is the saturated vapor density, that is itself dependent on temperature. This relationship is used in the vapor diffusion law that is based on Fick's law in a tortuous medium:

$$\mathbf{i_v}=-D\tau n\left(1-S_r\right)\mathbf{grad}\left(\rho_v\right) \tag{7}$$

where $\mathbf{i_v}$ is the vapor flow, D is the diffusion coefficient and τ the tortuosity.

It is then possible to distinguish the terms linked to the water pressure gradient from those linked to the temperature gradient in the gradient of vapor density, assuming the gradient of liquid water density is negligible:

$$\mathbf{grad}\left(\rho_v\right)=-\frac{\rho_v}{\rho_w R_v T}\mathbf{grad}\left(s\right)+\left[\frac{\rho_v}{\rho_{v,sat}}\frac{\partial\rho_{v,sat}}{\partial T}+\frac{\rho_v s}{\rho_w R_v T^2}\right]\mathbf{grad}\left(T\right) \tag{8}$$

This relationship shows the ability of the model to reproduce the transport of water vapor caused independently by suction and temperature gradients.

2.2.2. Heat diffusion

The energy balance equation of the mixture has the following form [8]:

$$\underbrace{\frac{\partial H}{\partial t}+L\frac{\partial}{\partial t}\left(\rho_v n\left(1-S_r\right)\right)}_{\text{Heat storage}}+\underbrace{div\left(\mathbf{f_T}\right)+L\cdot div\left(\mathbf{i_v}\right)}_{\text{Heat transfer}}-Q_T=0 \tag{9}$$

where H is the enthalpy of the whole medium, L the latent heat of water vaporization, $\mathbf{f_T}$ the heat flow and Q_T the volume heat source. Due to the assumption of thermal equilibrium, a single temperature is defined for solid, liquid and gas phases. The enthalpy can then be defined as the sum of the heat of each constituent:

$$H = \left[(1-n)\rho_s c_{p,s} + nS_r\rho_w c_{p,w} + n(1-S_r)\rho_v c_{p,v} + n(1-S_r)\rho_a c_{p,a}\right](T-T_r) \tag{10}$$

where ρ_s is the soil grain bulk density and $c_{p,w}$ $c_{p,s}$, $c_{p,a}$ and $c_{p,v}$ are the specific heat of liquid water, solid, dry air and water vapor, respectively. Heat transport is governed by conduction and convection:

$$\mathbf{f_T} = -\lambda \mathbf{grad}(T) + \left[c_{p,w}\rho_w \mathbf{f_l} + \left(c_{p,v} - c_{p,a}\right)\mathbf{i_v}\right](T-T_0) \tag{11}$$

where λ is the thermal conductivity of the mixture. Depending on the properties of each material, this physical characteristic is either considered as a function of the volume ratios of solid, liquid water and gas phases, or a specific function for the material. This distinction allows consideration of the specific evolution of bentonite thermal conductivity in relation to its degree of saturation.

In terms of couplings, it can be observed that both thermo-hydraulic and thermo-mechanical couplings are present through the evolution of the variables n and S_r.

2.3. Coupled mechanical constitutive model

2.3.1. Stress-strain framework

The mechanical part of the model that is used to describe the behavior of the buffer in this study, ACMEG-TS – Advanced Constitutive Model for Environmental Geomechanics – has already been the subject of investigations by François and Laloui. [5] and Dupray *et al.* [13]. The reader is directed to these papers for a more detailed overview of the model. Since focus of this paper is thermo-hydro-mechanical coupling, only the related aspects of the model are detailed in this section.

The behavior of the solid matrix is assumed to be governed by the generalized effective stress tensor $\boldsymbol{\sigma'}$ through a combination of total stress and fluid pressures [14]:

$$\boldsymbol{\sigma}' = \boldsymbol{\sigma} - p_g\mathbf{I} + S_r\left(p_g - p_w\right)\mathbf{I} \tag{12}$$

The term ($\boldsymbol{\sigma}$-$p_g\mathbf{I}$) is called the net stress, while (p_g-p_w) is the matrix suction s. The Lagrangian approach is used in the model, with the small strain deformation theory. The importance of using the generalized effective stress theory is to encompass most effects of suction in a single equation [15], which is important in hydro-mechanical coupling.

An important part of the thermo-mechanical coupling lies in the definition of strain, due to the phenomenon of thermal expansion. The following description of thermo-elasto-plastic strains is used:

$$d\boldsymbol{\varepsilon} = \mathbf{E}^{-1}d\boldsymbol{\sigma}' + \frac{\beta_s}{3}\mathbf{I}dT + d\boldsymbol{\varepsilon}^{\mathbf{p}} \tag{13}$$

where $d\boldsymbol{\varepsilon}$ is the total strain tensor increment, $\mathbf{E}$ the current non-linear elastic tensor, β_s the volumetric thermal expansion coefficient and $d\boldsymbol{\varepsilon}^{\mathbf{p}}$ the plastic strain tensor increment. The role of possible plastic strains on a thermal loading path where $d\boldsymbol{\sigma}'$ is null is evident in this equation. An important feature that derives from equations (12) and (13) is the behavior during a suction decrease at constant volume and constant temperature, or the unsaturated isothermal swelling pressure test path, which is described by this relation:

$$d\boldsymbol{\sigma} = -d(S_r s)\mathbf{I} - \mathbf{E}d\boldsymbol{\varepsilon}^{\mathbf{p}} \tag{14}$$

It can be noted that in the absence of plastic strains, the development of swelling pressure depends entirely on the increment of the product of suction and degree of saturation. This highlights the mechanical influence of the choice of the water retention behavior. It also shows that along a complete swelling pressure loading path, the manner in which plastic strains develop is also critical to the description of the swelling pressure development. Together with the influence of suction and temperature on the plastic behavior, which have been treated in detail in [5, 16, 17], these constitute the most intricate elements of the thermo-hydro-mechanical coupling.

2.3.2. Water retention model

The water retention behavior that is used in this study aims at representing at best the couplings observed in experiments on bentonite rather than focusing on a better representation of a one-directional wetting or drying path. It has been observed that temperature has a measurable effect on the relationship between the degree of saturation and suction, inducing a decrease in the degree of saturation for a constant suction [18]. The effect of dry density changes, which are linked to volumetric strain, is also well-known [19, 20]. A complete water retention behavior model should also include the hysteresis between drying and wetting paths.

The water retention model is shown in modeling. Two different yield limits in the (S_r–s) plane are activated depending on the direction of the loading, as long the suction is higher than the air entry value:

$$\begin{cases} f_{dry} = s - s_d = 0 \\ f_{wet} = s_{hys}s_d - s = 0 \end{cases} \tag{15}$$

where s_d is the drying yield limit and s_{hys} the parameter describing the size of the hysteresis.

The expression of the drying yield limit contains the coupled aspects of the formulation:

$$s_d = s_{e0}\exp\left(-\beta_h\ \Delta S_r\right)\left[1-\theta_T\log\left(T/T_0\right)-\theta_e\log\left(1-\varepsilon_v\right)\right] \tag{16}$$

where s_{e0} is the initial air entry value of the saturated material, β_h the slope of the desaturation curve in the (S_r–s) plane at constant volume and temperature, θ_T and θ_e are material parameters describing the evolution of air-entry suction with respect to temperature and volumetric strain, respectively.

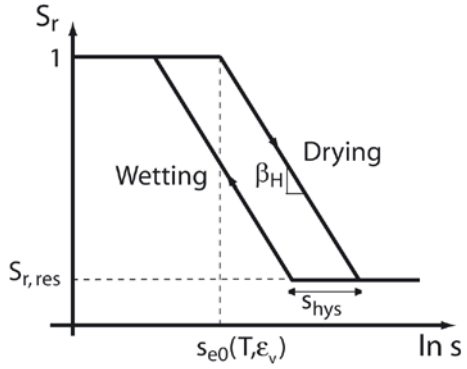

Fig. 2. : Schematic representation of water retention modeling.

2.3.3. THM plastic formulation

It is beyond the scope of this paper to fully describe the plasticity model that is used here, which is given in François and Laloui [5]. As the swelling behavior is fundamental in the response of the buffer of an EBS, only some elements of the isotropic behavior will be analyzed, emphasis on THM couplings. The coupling equation is based on the use of preconsolidation pressure as the main variable:

$$p'_c = \begin{cases} p'_{c0}\exp\left(\beta\ \varepsilon_v^p\right)\left[1-\gamma_T\log\left(T/T_r\right)\right] & \text{if } s \le s_e \\ p'_{c0}\exp\left(\beta\ \varepsilon_v^p\right)\left[1-\gamma_T\log\left(T/T_r\right)\right]\left[1+\gamma_s\log\left(s/s_e\right)\right] & \text{if } s \ge s_e \end{cases} \tag{17}$$

where p'_{c0} is the saturated initial preconsolidation pressure at the reference temperature T_r; β is the plastic compressibility modulus, defined as $\beta = \beta_m + \Omega.s$ (β_m being the plastic compressibility in saturated conditions) and γ_T and γ_s are material parameters. Since the shape of the initial yield surface is defined by the value of the effective preconsolidation pressure, the isotropic part of the yield surface is well represented by this value. In Fig. 3, the evolution of preconsolidation pressure with suction and temperature is represented. A decrease of this value with increasing temperature allows the creation of plastic strains in a purely thermal loading, thus representing the phenomenon of thermal collapse. A decrease in the suction will lead to the pressure reaching the yield surface, thus representing wetting collapse.

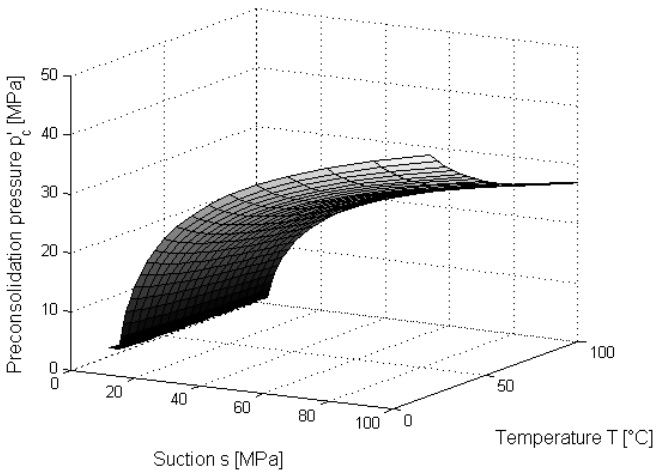

Fig. 3. Effect of temperature and suction on preconsolidation pressure (or isotropic yield limit).

3. CASE STUDY CHARACTERISTICS

3.1. Material characteristics

It is necessary to describe the two materials in this case study: the host rock and the buffer material. The rock is modeled as granite, with the objective that it does not directly control the water supply to the unsaturated buffer, inducing a relatively high intrinsic permeability of 10^{-17} m2. The other characteristics, such as porosity, bulk and shear modulus, heat capacity, thermal conductivity are derived from both in situ and laboratory measurements [21-23]. The rock is initially saturated but comes in contact with a high suction material during the test. Therefore, it may desaturate and, through changes in relative permeability, influence the resaturation process. Based on the findings of Finsterle and Pruess [24], a van Genuchten function is used to describe the retention behavior of granite, and its associated function for relative permeability:

$$S_w = \left(1+\left(s/P_r\right)^{1/(1-m)}\right)^{-m} \tag{18}$$

$$k_{r,w} = \sqrt{S_w}\left(1-\left(1-S_w^{\,1/m}\right)^m\right)^2 \tag{19}$$

where m and P_r are a material parameter and a reference pressure, respectively. Mechanically, the host rock is considered as a linear elastic material in the classical effective stress framework.

The buffer is made of highly compacted MX-80 bentonite blocks. These blocks have a saturated density of 2000 kg/m^3. The initial degree of saturation is 0.61, corresponding to a suction of 48 MPa. A base case is considered, using parameters that are derived from those used in [25] and adapted to the previously described constitutive model. Variations in some of the parameters are then considered to perform the analysis of THM

couplings in the buffer. The parameters for the base case of the constitutive equations presented in sections 2.2 and 2.3 are summarized in Table 1. Some empirical relationships of the model were not treated directly as a part of the constitutive model and are detailed here. The relative permeability description of the rock is crucial, and a power law is used [26]:

$$k_{r,w} = S_w^{\ 3} \tag{20}$$

The specifics of the changes in bentonite thermal conductivity during changes in the degree of saturation also lead to the use of an empirical law that best describes the results gathered in [25]:

$$\lambda = \lambda_{sat} - \frac{\lambda_2}{1+\exp\left((S_w - S_3)/S_4\right)} \tag{21}$$

Table 1. Parameters used in the base case simulation for both bentonite and granite

Thermal parameters	Bentonite	Granite
Saturated thermal conductivity [W/m/K]	1.3	-
Thermal conductivity parameter λ_2 [W/m/K]	1.04	-
" S_3 [-]	0.52	-
" S_4 [-]	0.12	-
Solid thermal conductivity [W/m/K]	-	2.4
Water thermal conductivity [W/m/K]	-	1.18
Air thermal conductivity [W/m/K]	-	0
Solid heat capacity [J/kg/K]	800	770
Water heat capacity [J/kg/K]	4183	4183
Air heat capacity [J/kg/K]	1000	1000
Solid thermal expansion coefficient [K^{-1}]	1.02×10^{-5}	2.16×10^{-5}
Water thermal expansion coefficient[K^{-1}]	3.4×10^{-4}	3.4×10^{-4}
Flow parameters		
Intrinsic permeability [m^2]	6.4×10^{-21}	1×10^{-17}
Kozeny-Carman parameter [-]	5.33	-
Relative permeability parameter m [-]	-	0.6
Relative permeability parameter P_r [MPa]	-	1.74
Initial porosity [-]	0.438	0.003
Tortuosity [-]	1	1
Other parameters		
Solid specific mass [kg/m^3]	2780	2700
Water specific mass [kg/m^3]	1000	1000
Air specific mass [kg/m^3]	1.18	1.18
Isothermal water compressibility [Pa^{-1}]	0	0
Mechanical parameters		
Young's modulus [GPa]	see Table 2	62
Poisson's ratio [-]	0.2	0.24

As stated earlier, the constrained swelling response of the buffer is crucial to the mechanical behavior of the whole EBS design. The dry density of the buffer considered here leads to a design swelling pressure of 5.21 MPa. This value, along with the saturated elastic modulus of 20 MPa allows the determination of a set of parameters for the isothermal unsaturated behavior of the buffer in the ACMEG-TS model, as explained in [13]. These parameters are shown in Table 2.

Table 2. Set of ACMEG-TS parameters for the base case simulation (see [5])

Elastic parameters		
K_{ref}, G_{ref}, n^e	[MPa], [MPa], [-]	22.2, 16.7, 1
Isotropic plastic parameters		
β, γ_s, γ_T, r^e_{iso}, p'_c, Ω	[-], [-], [-], [-], [MPa], [-]	30, 8, 0.2, 0.7, 1.5, 10^{-6}
Deviatoric plastic parameters		
b, d, ϕ', g, α, a, r^e_{dev}	[-], [-], [°], [-], [-], [-], [-]	0.1, 2, 30, 0, 1, 0.001, 0.8
Water retention parameters		
s_{e0}, β_h, θ_T, θ_e, s_{hys}	[MPa], [-], [-], [-], [-]	3, 7, 0, 0, 0

3.2. Simulation characteristics

The model consists of 2211 8-node elements and is run as an axisymmetric model. Apart from the geometry of the problem that was defined in the introduction, it is necessary to describe the loading path of the simulation. The initial equilibrium is obtained by the application of forces along the empty hole. In a first stage, the considered hole is excavated by releasing those forces. A 100 % humidity rate is then applied in the hole for 30 days. The operational stage of the EBS is finally simulated through the introduction of a heat-emitting canister and its surrounding buffer material. The canister emits heat at an initial rate of 1700 W, with a progressive decay that can be seen in Table 3, derived from the work of Hökmark *et al.* [27]. The canister itself, though not described previously, is modeled as a continuous material described by linear thermo-elasticity, with a Young's modulus of 180 GPa, a Poisson's ratio of 0.3 and a volumetric thermal expansion coefficient of 5.1×10^{-5} K^{-1}.

Table 3. Simulated heat decay of the canister

Time [yr]	Power [W]
0	1700
1	1671
10	1416
20	1232
50	828
100	520
1000	109

4. BASE CASE AND SENSITIVITY

4.1. Base case description

This section presents the values that will serve as a reference for the analysis of variations in the buffer behavior. The chosen values are the maximum temperature, the maximum suction, the resaturation time and the swelling pressure. These values all correspond to a design criteria of EBS, and as such appear as the most relevant for a sensitivity analysis. They are monitored at 7 locations as shown in Fig. 1: three points are at the level of the middle of the canister, three are 75 cm above the canister and one is on top of the canister.

With regard to temperature, a value of 79 °C is reached 20 years after emplacement in location P22. The temperature evolution at all points is given in Fig. 4, which shows the buffer effect of the bentonite gap in terms of maximum temperature and the corresponding time delay for points 75 cm above the canister.

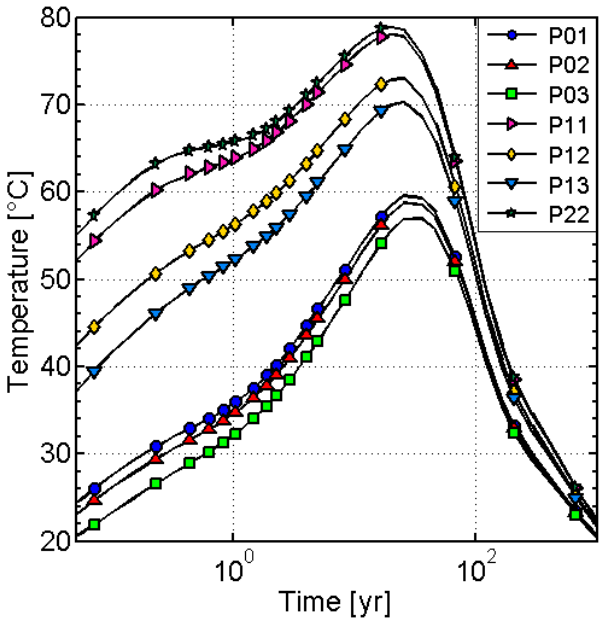

Fig. 4. Temperature evolution in the buffer (base case).

Fig. 5shows the evolution of pore pressure in the buffer in the first years, mainly in the negative values (suction). The locations close to the canister are affected by an increase in suction, reaching more than 120 MPa on top of the canister and more than 60 MPa on the side, starting from 49 MPa. The evolution of the degree of saturation shown in Fig. 6 is another sign of the same phenomenon, with the degree of saturation going below 0.5 at the top of the canister. The resaturation time is 4.1 years on the sides, but 5.3 years on the top.

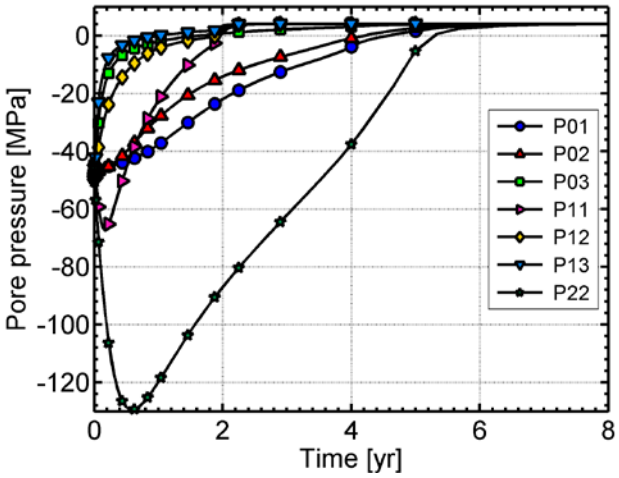

Fig. 5. Pore water pressure evolution in the buffer (base case).

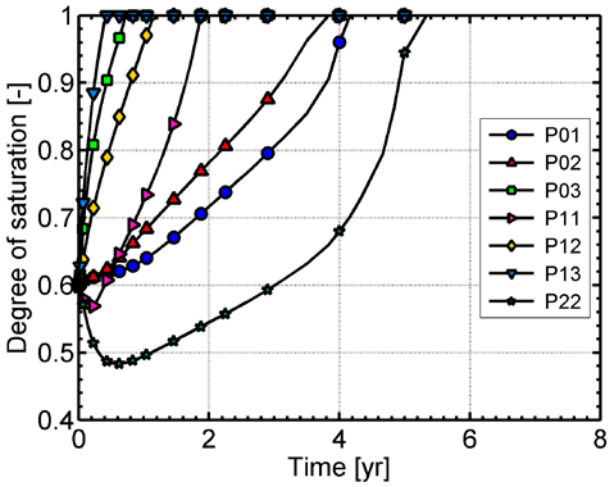

Fig. 6. Degree of saturation evolution in the buffer (base case).

Fig. 7 shows the same process of pore pressure evolution but in the host rock. The influence of excavation is shown in negative times. The contact between unsaturated bentonite and rock is shown to be important only during a very brief period. This is also highlighted in Fig. 8 which shows the degree of saturation through a horizontal rock profile at the beginning. Desaturation only occurs in the first 1.5 m of rock and for 2 days. After about 1 year pore pressures are back to their initial level, and the slight increase that can be seen is attributed to thermal effects. It peaks at three years and is here limited to 60 kPa.

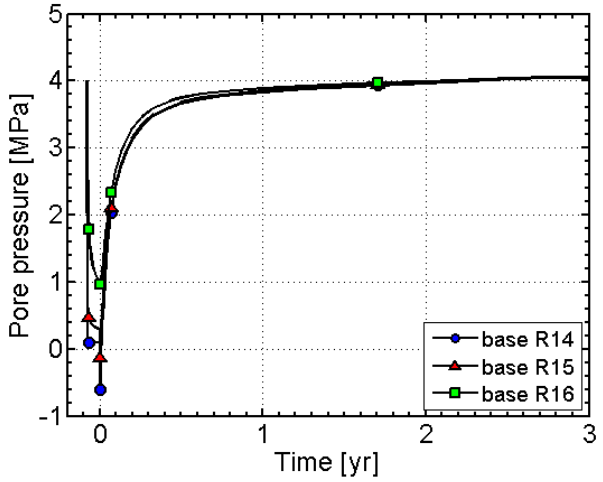

Fig. 7. Pore water pressure evolution in the host rock (base case). Negative times correspond to excavation period.

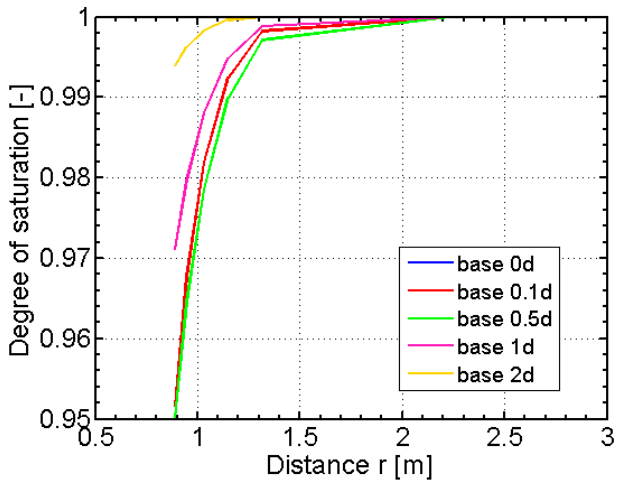

Fig. 8. Degree of saturation in the rock close to the excavation during bentonite emplacement.

Fig. 9 and Fig. 10 present the evolution of both the mean effective stress and mean mechanical stress (or swelling pressure), the swelling stress tensor being defined as $\boldsymbol{\sigma}_{sw} = \boldsymbol{\sigma}' + S_r s \mathbf{I}$. Two main effects are visible: drying shrinkage and final swelling pressure. Drying shrinkage is visible (as tensile net stresses) in the aforementioned areas close to the canister, most notably on top of it. Tensile stresses are obtained due to the perfect bonding that is assumed between elements in the simulation, used instead of modeling the gaps necessary for construction. This simplification may affect local results on top of the canister but does not significantly affect other factors of the simulation as the main real gap (between blocks and host rock) is quickly filled by swelling bentonite saturated from water inflow from granite. The final swelling pressure establishes itself between 5.2 and 6.9 MPa in all locations, highlighting the sealing capacity of the buffer. This is close to the design value of 5.25 MPa.

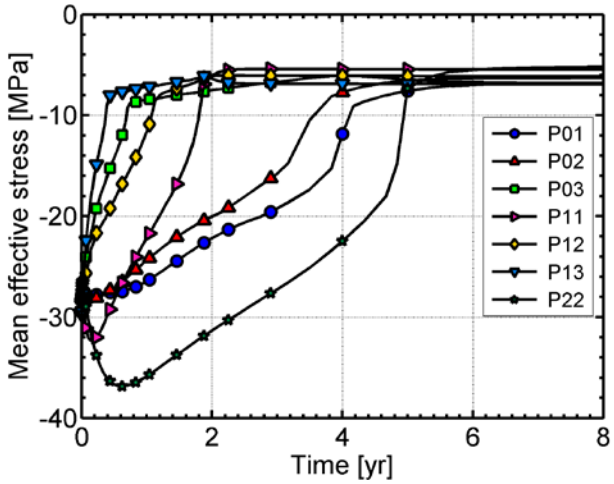

Fig. 9. Mean effective stress evolution in the base case.

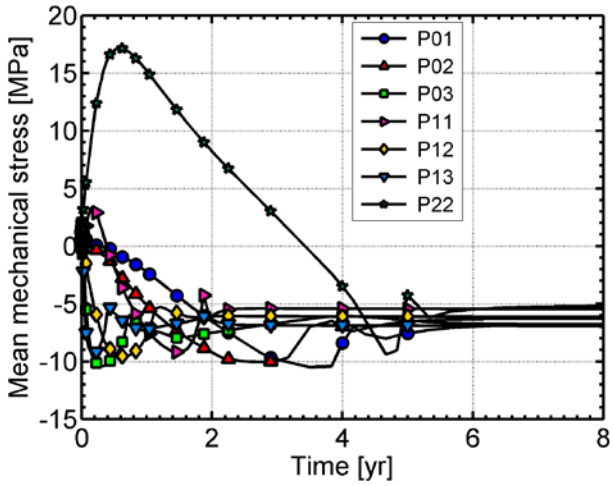

Fig. 10. Swelling pressure evolution in the base case.

4.2. Effect of rock permeability

One of the main aspects related to the host rock that may influence the processes in the buffer in terms of resaturation, temperature… is thought to be rock permeability. In order to quantify this effect, three permeabilities were assessed around the base case value of 10^{-17} m^2: 10^{-15} and 10^{-19} m^2. Fig. 11 shows the changes in pore pressures in the host rock in the short term (10 years), where the effect of a low permeability rock is especially obvious. The high permeability rock shows limited changes to the base case, only reaching a stable state similar to the natural state faster than in the base case, and showing no thermal overpressure. The low permeability rock pore pressure is also still growing after 10 years due to thermal overpressures, and this in fact goes up to 6.5 MPa, or 2.5 MPa overpressure. This phenomenon lasts for about 40 years, and the resistance of such rock against this type of loading should be investigated.

The low permeability rock desaturates notably but on a limited depth. This desaturated layer then also acts as an

almost impermeable layer and delays the water ingress in the buffer area. The cause for this effect lies in the relative water permeability law, and is highlighted in Fig. 12, which shows the hydraulic conductivity in this layer going down to 10^{-18} m/s. Only after 6 years does it reach a saturated state. This timeframe corresponds precisely to the resaturation period of the buffer, and the coupling between this time and not only host rock permeability, but also relative permeability description, becomes obvious.

Fig. 13 finally shows the result of this coupling, with the increase in resaturation time at various points in the buffer. The low permeability case creates an increase of 4 years in resaturation time, but also in the meantime, the suction state in the buffer goes to a much higher level than in the base case, which can then go beyond design values. On the other hand, the effect of a high permeability rock is hardly visible and shows that under given conditions, the buffer itself is controlling fully the resaturation time.

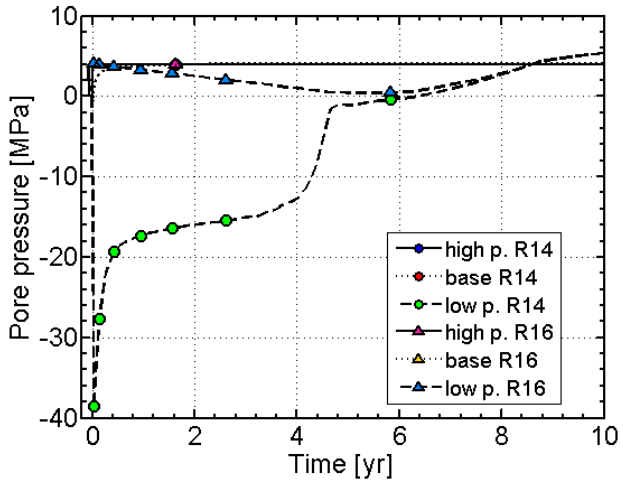

Fig. 11. Evolution of pore pressures in the rock for 3 different rock permeabilities.

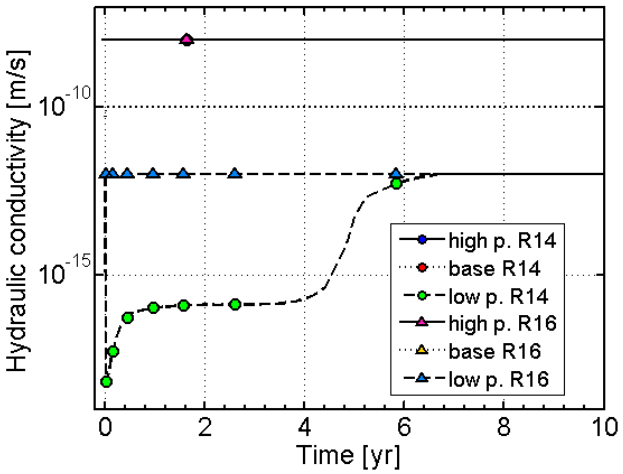

Fig. 12. Hydraulic conductivities in the rock for the three cases.

Another aspect is the evolution of stresses in the host rock during the timeframe that is considered for nuclear waste storage, more than 1000 years. The present model, being axisymmetric with symmetry boundary represents correctly a hexagonal pattern of vertical drifts for canisters. Rock located between the drift is therefore highly constrained laterally. Such aspect is obvious in Fig. 14, which shows horizontal total stress in the rock. The global shape of the curve is governed by temperature evolution, the time of peak stress corresponding to the time of peak temperature. Nevertheless, significant variations are observed between the three cases, especially between low permeability rock and the base case, and they are not all related to pure rock behavior. The development of swelling pressure in the buffer is especially visible at point R14 (on the excavation surface), and the delay with which it develops in the low permeability case is visible. Peak values are also about 6 % higher in that case than in the base case.

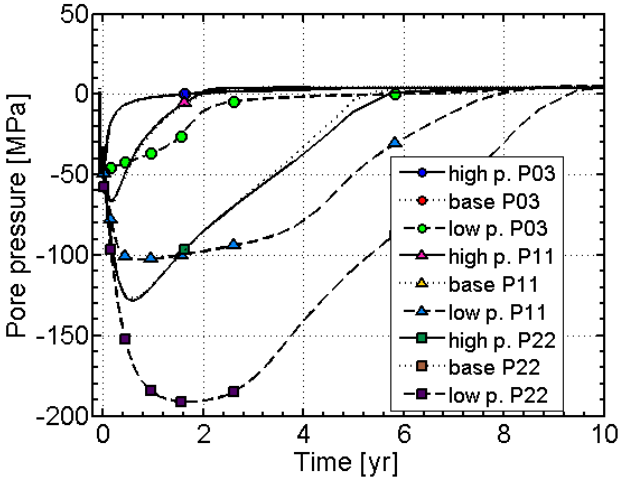

Fig. 13. Evolution of pore pressures in the buffer for 3 different rock permeabilities.

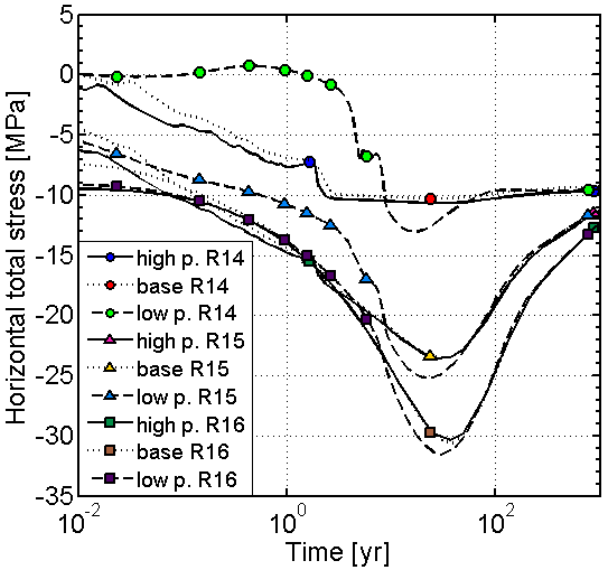

Fig. 14. Evolution of total horizontal stress in the rock for 3 different rock permeabilities.

5. CONCLUSIONS

This paper investigates some aspects of the description and parameterization of host rock behavior in the global response of an EBS, while using advanced models for the buffer part of the problem. Through a case study based on the Swedish design, with a maximum temperature of around 80 °C, the effect of rock permeability and water retention behavior have been highlighted. The answers that come with the paper are aimed at improving the measurement program regarding candidate sites depending on their characteristics. It is shown that for comparatively high (above 10^{-17} m^2) permeabilities, the buffer is controlling all aspects linked to resaturation (time, swelling pressures, transient temperatures), therefore in those cases, careful investigations into the hydraulic characteristics of the rock are deemed less useful. On the other hand, for low permeabilities, intricate aspects of thermo-hydraulic couplings are shown to strongly influence buffer response, as well as rock stresses. The value of permeability itself becomes only one of the factors that need to be determined properly and that all strongly affect the response: water retention behavior of the rock, and relative permeability in unsaturated conditions. Further aspects will also be studied in the presented framework, such as effects of porosity, water retention curves.

6. ACKNOWLEDGMENTS

The authors would like to acknowledge the participation of NAGRA in this project and the help from SKB through EBS-Task Force, and personally A. Schäfers from BGR.

REFERENCES

1. Iaea. 2006. International Atomic Energy Agency: Geological disposal of Radioactive Waste. Safety Requirements, IAEA Safety Standards Series No. WS-R-4.

2. Nagra. 2002. Project Opalinus Clay: Safety Report. Demonstration of disposal feasibility (Entsorgungsnachweis) for spent fuel, vitrified high-level waste and long-lived intermediate-level waste, Technical Report NTB 02-05, NAGRA.

3. Skb. 2011. Long term test of buffer material at the Äspö HRL, LOT project, Technical Report TR-09-31, SKB, 123 p.

4. Laloui, L., B. François, M. Nuth, H. Péron, and A. Koliji. 2008. A thermo-hydro-mechanical stress-strain framework for modeling the performance of clay barriers in deep geological repositories for radioactive waste. Keynote paper in *1st European Conf. on Unsaturated Soils*. Durham, UK. 63-80.

5. François, B. and L. Laloui. 2008. ACMEG-TS: A constitutive model for unsaturated soils under non-isothermal conditions. *International Journal for Numerical and Analytical Methods in Geomechanics*. 32(16):1955-1988.

6. Bowen, R.M. 1982. Compressible porous media models by use of the theory of mixtures. *International Journal of Engineering Science*. 20(6):697-735.

7. Panday, S. and M.Y. Corapcioglu. 1989. Reservoir transport equations by compositional approach. *Transport in Porous Media*. 4(4):369-393.

8. Collin, F., X.L. Li, J.P. Radu, and R. Charlier. 2002. Thermo-hydro-mechanical coupling in clay barriers. *Engineering Geology*. 64(2-3):179-193.

9. Börgesson, L., M. Chijimatsu, T. Fujita, T.S. Nguyen, J. Rutqvist, and L. Jing. 2001. Thermo-hydro-mechanical characterisation of a bentonite-based buffer material by laboratory tests and numerical back analyses. *International Journal of Rock Mechanics and Mining Sciences*. 38(1):95-104.

10. Wang, W., J. Rutqvist, U.-J. Görke, J. Birkholzer, and O. Kolditz. 2011. Non-isothermal flow in low permeable porous media: a comparison of Richards' and two-phase flow approaches. *Environmental Earth Sciences*. 62(6):1197-1207.

11. Villar, M.V. and A. Lloret. 2004. Influence of temperature on the hydro-mechanical behaviour of a compacted bentonite. *Applied Clay Science*. 26(1-4):337-350.

12. Thomas, H.R. and S.D. King. 1994. A non-linear, two-dimensional, potential-based analysis of coupled heat and mass transfer in a porous medium. *International Journal for Numerical Methods in Engineering*. 37(21):3707-3722.

13. Dupray, F., B. François, and L. Laloui. 2013. Analysis of the FEBEX multi-barrier system including

thermoplasticity of unsaturated bentonite. *International Journal for Numerical and Analytical Methods in Geomechanics*. 37(4):399-422.

14. Laloui, L. and M. Nuth. 2009. On the use of the generalised effective stress in the constitutive modelling of unsaturated soils. *Computers and Geotechnics*. 36(1–2):20-23.
15. Nuth, M. and L. Laloui. 2008. Effective stress concept in unsaturated soils: Clarification and validation of a unified framework. *International Journal for Numerical and Analytical Methods in Geomechanics*. 32(7):771-801.
16. Cekerevac, C. and L. Laloui. 2004. Experimental study of thermal effects on the mechanical behaviour of a clay. *International Journal for Numerical and Analytical Methods in Geomechanics*. 28(3):209-228.
17. Hueckel, T., B. François, and L. Laloui. 2009. Explaining thermal failure in saturated clays. *Géotechnique*. 59(3):197-212.
18. Romero, E., A. Gens, and A. Lloret. 2001. Temperature effects on the hydraulic behaviour of an unsaturated clay. *Geotechnical and Geological Engineering*. 19(3):311-332.
19. Nuth, M. and L. Laloui. 2008. Advances in modelling hysteretic water retention curve in deformable soils. *Computers and Geotechnics*. 35(6):835-844.
20. Gallipoli, D., S.J. Wheeler, and M. Karstunen. 2003. Modelling the variation of degree of saturation in a deformable unsaturated soil. *Géotechnique*. 53(1):105-112.
21. Maaranen, J., J. Lehtioksa, and J. Timonen. 2001. Determination of porosity, permeability and diffusivity of rock samples from Äspö HRL using the helium gas method, International Progress Report IPR-02-17, SKB.
22. Makurat, A., F. Løset, A. Wold Hagen, L. Tunbridge, V. Kveldsvik, and E. Grimstad. 2006. A descriptive rock mechanics model for the 380–500 m level, Report R-02-11, SKB.
23. Sundberg, J. 2002. Determination of thermal properties at Äspö HRL, Report R-02-27, SKB, 66 p.
24. Finsterle, S. and K. Pruess. 1995. Solving the Estimation-Identification Problem in Two-Phase Flow Modeling. *Water Resources Research*. 31(4):913-924.
25. Åkesson, M., L. Börgesson, and O. Kristensson. 2010. SR-Site Data report: THM modelling of buffer, backfill and other system components, Technical Report TR-10-44, SKB, 98 p.
26. Vaunat, J. and A. Gens. 2005. Analysis of the hydration of a bentonite seal in a deep radioactive waste repository. *Engineering Geology*. 81(3):317-328.
27. Hökmark, H., M. Lönnqvist, and B. Fälth. 2008. Rock Mechanics Issues in the Swedish Waste Management Program. Keynote paper in *The 42nd U.S. Rock Mechanics Symposium (USRMS)*. San Francisco, CA: American Rock Mechanics Association.